Colloids and Surfaces B: Biointerfaces 141 (2016) 158–169

Contents lists available at ScienceDirect

Colloids and Surfaces B: Biointerfaces

journal homepage: www.elsevier.com/locate/colsurfb

Silver nanoparticles synthesized from *Adenium obesum* leaf extract induced DNA damage, apoptosis and autophagy *via* generation of reactive oxygen species

Mohammad Abul Farah[a,*,1], Mohammad Ajmal Ali[b,1], Shen-Ming Chen[c], Ying Li[c], Fahad Mohammad Al-Hemaid[b], Faisal Mohammad Abou-Tarboush[a], Khalid Mashay Al-Anazi[a], Joongku Lee[d]

[a] *Department of Zoology, College of Science, King Saud University, Riyadh 11451, Saudi Arabia*
[b] *Department of Botany and Microbiology, College of Science, King Saud University, Riyadh 11451, Saudi Arabia*
[c] *Department of Chemical Engineering and Biotechnology, National Taipei University of Technology, No.1, Section 3, Chung-Hsiao East Road, Taipei 106, Taiwan, ROC*
[d] *Department of Environment and Forest Resources, Chungnam National University, 99 Daehak-ro, Yuseong-gu, Daejeon 34134, Republic of Korea*

ARTICLE INFO

Article history:
Received 4 November 2015
Received in revised form 12 January 2016
Accepted 15 January 2016
Available online 18 January 2016

Keywords:
Silver nanoparticles
Adenium obesum
Comet assay
Apoptosis
Autophagy
Reactive oxygen species

ABSTRACT

Silver nanoparticles (AgNPs) are an important class of nanomaterial used for a wide range of industrial and biomedical applications. *Adenium obesum* is a plant of the family Apocynaceae that is rich in toxic cardiac glycosides; however, there is scarce information on the anticancer potential of its AgNPs. We herein report the novel biosynthesis of AgNPs using aqueous leaf extract of *A. obesum* (AOAgNPs). The synthesis of AOAgNPs was monitored by color change and ultraviolet–visible spectroscopy (425 nm). It was further characterized by Fourier transform infrared (FTIR) spectroscopy, X-ray diffraction (XRD) and transmission electron microscopy (TEM). The FTIR spectra for the AOAgNPs indicated the presence of terpenoids, long chain fatty acids, secondary amide derivatives and proteins that could be responsible for the reduction and capping of the formed AOAgNPs. X-ray diffraction confirmed the crystallinity of the AgNPs. The TEM images revealed mostly spherical particles in the size range of 10–30 nm. The biological properties of novel AOAgNPs were investigated on MCF-7 breast cancer cells. Cell viability was determined by the MTT assay. Generation of reactive oxygen species (ROS), DNA damage, induction of apoptosis and autophagy were assessed. A dose-dependent decrease in the cell viability was observed. The IC_{50} value was calculated as 217 μg/ml. Both qualitative and quantitative evaluation confirmed about a 2.5 fold increase in the generation of ROS at the highest concentration of 150 μg/ml. A significant ($p < 0.05$) increase in the DNA damage evaluated by comet assay was evident. Flow cytometry revealed an increase in the apoptotic cells (24%) in the AOAgNPs treated group compared to the control. Acridine orange staining of acidic vesicles in exposed cells confirmed the induction of autophagy. These findings suggest that AOAgNPs increased the level of ROS resulting in heightened the DNA damage, apoptosis and autophagy in MCF-7 cells.

1. Introduction

Nanoparticles (NPs) are small sized (1–100 nm) compounds that are becoming widespread in consumer products and medical applications. The nature and unique properties of NPs means that they have a wide range of applications, such as in therapeutic compounds, transfection vectors, anti-microbial agents, fluorescent labels, deoxyribonucleic acid (DNA) modification, drug delivery systems, cosmetics and medical devices [1,2]. Silver nanoparticles (AgNPs) are the most commercialized and prominent group of nano-compounds due to their diverse applications in the health sector. Recently, various attempts have been made to use AgNPs as anticancer agents with positive outcomes [3,4]. The mechanisms for AgNPs induced toxicity may be related to the production of excess reactive oxygen species (ROS). The production of ROS and AgNPs induced DNA damage has previously been reported in HeLa cells [5], and several other studies have revealed that AgNPs induce mitochondrial damage, DNA damage, apoptosis, oxidative stress and impairment of nuclear DNA [6,7].

* Corresponding author.
E-mail addresses: farahabul@hotmail.com, mfarah@ksu.edu.sa (M.A. Farah).
[1] The first and second authors provided an equal contribution to this paper.

http://dx.doi.org/10.1016/j.colsurfb.2016.01.027
0927-7765/

A number of approaches are available for the synthesis of AgNPs. For example, AgNPs can be synthesized by chemical, electrochemical, radiation, photochemical and biological methods [8–11]. Due to their environmental impact, energy consumption, and use of toxic chemicals, however, a green approach to the synthesis of AgNPs is preferable [12,13]. The green synthesis of AgNPs has previously been reported from a wide range of plants [14] including some important medicinal plants of the family Apocynaceae such as *Calotropis procera* [15] and *Nerium indicum* [16]. Moreover, some of the recent reports demonstrate that AgNPs synthesized using the green approach, such as from *Phyllanthus emblica, Albizia adianthifolia, Annona squamosa* and *Chrysanthemum indicum*, have cytotoxic effects against various cell lines [17–20].

Adenium obesum (Forssk.) Roem. & Schult. (family Apocynaceae), commonly known as 'Desert Rose' is primarily an ornamental plant. All parts of this plant (including latex) are used in traditional medicines for the treatment of skin lumps, wounds, earache, rhinitis, gonorrhoea and infectious diseases. It is also a poisonous plant, and therefore used as a pesticide [21]. Previous phytochemical studies on *A. obesum* have revealed that it contains toxic cardiac glycosides (cardenolides), pregnanes, triterpenes, flavonoids and carbohydrate [22]. The extract of the aerial part of *A. obesum* has previously been reported to have cytotoxic [23] and anti-influenza activities [24].

Cancer is characterized by invasive and uncontrolled cell division and the spread of abnormal cells [25]. Each year 6.7 million people worldwide die from different types of cancer. Female breast cancer is the most common malignant disease among women in developed, as well as in developing countries [26]. Chemotherapy and radiotherapy used for the treatment of cancer have serious and well-known side effects, such as nausea, anaemia, leukopenia, neutropenia, asthenia and low immunity [27]. The alternative treatment options are very limited due to their resistance to conventional chemotherapy and radiotherapy. Although there are a wide range of cytotoxic agents used in the treatment of breast cancer, such as doxorubicin, cisplatin and bleomycin, there are various drawbacks in their use and they are not very efficient [28]. Developing a biocompatible and more effective method for the treatment of cancer using nanotechnology and natural products is of great interest, therefor.

In this study, the novel, one-step biosynthesis of AgNPs using the leaf extract of *A. obesum* at room temperature has been reported for the first time. The objective of this study is to synthesize AgNPs using a green synthesis method, and to characterize the AgNPs using ultraviolet–visible spectroscopy (UV–vis), Fourier transform infrared (FTIR) spectroscopy, X-ray diffraction (XRD) and transmission electron microscopy (TEM). In addition, we have made an attempt to evaluate its anticancer potential by elucidating cytotoxic and genotoxic effects on human breast cancer (MCF-7) cells. A comparison of biosynthesized AgNPs cytotoxicity with crude leaves extract and commercial AgNPs has also been made. Since ROS generation has been shown to play an important role in apoptosis induced by AgNPs [29,30], this study used 2,7-dichlorfluorescein-diacetate (DCFH-DA) assay to determine whether ROS generation could be a possible mechanism in the observed cytotoxicity of AOAgNPs. ROS has also been shown to regulate autophagy, a physiologically regulated catabolic process, which is not only involved in energy homeostasis, organelle turnover and development, but also in cancer cell death [31]. The comet assay is a promising technique that has been applied mainly to the study of single-strand DNA breaks induced by a variety of toxic agents, including chemical compounds, ionizing radiation and nanoparticles in cells [32,33]. Thus, in the present study, we employed a well characterized AOAgNPs which provide a unique opportunity to investigate the mechanisms of DNA damage, apoptosis and autophagy induced in MCF-7 cells through ROS generation.

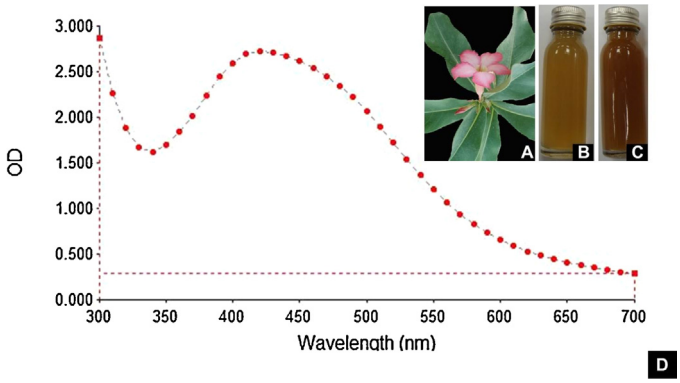

Fig. 1. The ultraviolet–visible spectra of *A. obesum* silver nanoparticles (AOAgNPs). The absorption spectra of AOAgNPs exhibited a strong broad peak at 425 nm (D). The inset shows a twig of *A. obesum* (A), and the synthesis of AOAgNPs using the leaf extract from *A. obesum* (B,C). (B) The photo shows a container with a solution of 1 mM $AgNO_3$ with aqueous leaf extract of *A. obesum*. After exposure for 120 min the color of the solution turned from slight yellowish to brown (C), indicating the green synthesis of AOAgNPs.

2. Materials and methods

2.1. Reagents and consumables

Minimum essential medium (MEM), fetal bovine serum (FBS), trypsin/EDTA and penicillin-streptomycin were purchased from Invitrogen (Carlsbad, CA, USA). Analytical-grade silver nitrate ($AgNO_3$), trypan blue, phosphate buffered saline (PBS), agarose (low melt), agarose (normal melt), NaCl, Na_2EDTA, tris, triton X-100, NaOH, dimethyl sulfoxide (DMSO), ethidium bromide, 2,7-dichlorofluorescin diacetate, acridine orange, doxorubicin and AgNPs were obtained from Sigma–Aldrich (St Louis, MO, USA). The physical characteristics of the AgNPs according to the manufacturers data are; size (≤100 nm), purity (99.5%), trace metal basis, surface area (5.0 m^2/g), density (10.49 g/cc). Annexin-V FITC apoptosis detection kit was procured from BD Biosciences (San Jose, CA, USA). Cell Titer 96® Non-radioactive cell proliferation assay kit was obtained from Promega (Madison, WI, USA). Culture wares and other plastic consumables used in this study were procured from Nunc, Denmark.

2.2. Biosynthesis and characterization of silver nanoparticles

The leaves of *A. obesum* (Fig. 1A) were collected from Riyadh, Saudi Arabia, and were identified by consulting the herbarium specimens housed at KSUH (Herbarium of King Saud University, Riyadh, Saudi Arabia). The collected leaf materials were rinsed thoroughly with tap water to remove extraneous contaminants and then cut into small pieces and oven-dried at 50 °C until the dry weight stabilized. The dried small pieces of leaves were then boiled in a 250-ml glass beaker along with 200 ml of Milli-Q deionized water (EMD Millipore, Billerica, MA, USA) for 10 min. The aqueous extract was separated by filtration with Whatman No. 1 filter paper (Maidstone, UK), and then centrifuged at 1,200 rpm for 5 min to remove heavy biomaterials. The extract was stored at room temperature to be used for the biosynthesis of silver nanoparticles from silver nitrate. An aqueous solution (1 mM) of $AgNO_3$ was prepared in 250 mL Erlenmeyer flasks, and aqueous extract was added for reduction into Ag+ ions. The reaction (99 ml 1 mM $AgNO_3$ + 1 ml aqueous leaf extract) was carried out in darkness in order to avoid photoactivation of $AgNO_3$ at room temperature. The reaction mixture was kept undisturbed until the slight yellowish solution converted into a brown color, which indicated the synthesis of AgNPs.

Characterization of NPs is essential in nanotoxicology research for a better interpretation of the results [34]. The changes in colour were therefore recorded along with periodic sampling and scanning by UV–visible spectrophotometry (BioTek, Winooski, VA, USA) in the wavelength ranging from 300–700 nm for a maximum of 120 min. Further, the reaction mixture was centrifuged at 10,000 rpm for 10 min and the pellet was dissolved in sterile distilled water and the AgNPs were washed three times by centrifugation to remove impurities. It was then lyophilized and stored in screw-capped vials under ambient conditions for further characterization and application. FTIR spectra of the samples were measured (PerkinElmer: model spectrum RXI) in the transmittable mode at the range of 4000–500 cm^{-1} in KBr pellets. Further, the crystalline structures of the synthesized AgNPs were investigated by XRD. Lyophilized and powdered samples were used, and the diffraction patterns were recorded in the scanning mode on an X'pert Pro diffractometer (PANalytical, Almelo, the Netherlands) operated at 40 kV and with a current of 30 mA, with Cu/kα radiation (λ = 1.5418 Å) in the range of 20–80° in 2θ angles. TEM was performed with a JEM 1101 transmission electron microscope (JEOL, Tokyo, Japan) to confirm the size and shape of the AOAgNPs. The sample was dispersed in ethanol on a carbon-coated copper TEM grid, and the images were obtained by operating at an accelerating voltage of 120 kV.

2.3. Cell culture and treatments

The MCF-7 human breast adenocarcinoma cell line was obtained from American Type Culture Collection (ATCC, Rockville, MD, USA). The cells were maintained in MEM with 15% FBS and 1% penicillin/streptomycin in a completely humidified atmosphere with 95% air and 5% CO_2 at 37 °C. Cells were grown as adherent monolayers in T-25 and T-75 culture flasks. The exponentially growing cells at 90–95% confluence were harvested using 0.25% trypsin/EDTA solution and sub-cultured into 6-well or 96-well plates according to the experimental requirements. The viability of the cells was determined by staining with trypan blue [35]. The cells were counted using a haemocytometer and diluted in medium at a density of 1×10^5 cells/ml to be used throughout the experiments. A stock solution of AOAgNPs and commercially procured AgNP was prepared in PBS at a concentration of 10 mg/ml (w/v) and was sonicated for 15 min in order to make a well-dissolved AOAgNPs solution. The stock solution was then diluted in culture medium to obtain the desired concentrations for cell treatment. Doxorubicin (DOX) was dissolved in complete cell culture medium at a concentration of 50 μM for use as a positive control.

2.4. Cytotoxicity assay

The 3-(4,5-dimethylthiazol-2-yl)-2,5-diphenyl tetrazolium bromide (MTT) colorimetric assay [36] with modification was used to analyze the cytotoxic activity of AOAgNPs. A CellTitre 96® non-radioactive cell proliferations assay kit (Promega, Madison, WI, USA) was used following the manufacturer's instructions. Briefly, the MCF-7 cells (1×10^4 cells/well) were grown overnight in 96-well flat bottom cell culture plates, and were then exposed to six different concentrations (600 μg/ml, 500 μg/ml, 400 μg/ml, 300 μg/ml, 200 μg/ml and 100 μg/ml) of AOAgNPs and crude aqueous leaf extract for 24 h. Cells were also exposed to six different concentrations of AgNPs (120 μg/ml, 100 μg/ml, 80 μg/ml, 60 μg/ml, 40 μg/ml and 20 μg/ml) for the same duration. In addition, negative/vehicle controls, and a positive control (DOX) were also used for comparison. After the completion of the desired treatment, 15 μl of MTT reagent, provided in the kit, was added to each well and further incubated for 3 h at 37 °C. Finally, the medium with MTT solution was removed, and 200 μl of solubilization solution was added to each well and further incubated for 30 min. The optical density (OD) of each well was measured at 550 nm by using a Synergy microplate reader (BioTek, Winooski, VA, USA). Results were generated from three independent experiments and each experiment was performed in triplicate. The percentage of cytotoxicity compared to the untreated cells was estimated in order to determine the IC_{50} value (the concentration at which 50% cell proliferation is inhibited).

2.5. Morphological changes analysis

Cells were seeded in a 6-well plate at a density of 1×10^5 cells per well and allowed to grow overnight. Morphological changes were observed to determine the alterations induced by AOAgNPs in MCF-7 cells treated with 50, 100 and 150 μg/mL concentration of AOAgNPs for 24 h. After the end of the incubation period, cells were washed with PBS (pH 7.4) and observed under a phase contrast inverted microscope equipped with a digital camera (Olympus IX51, Tokyo, Japan) at 100× magnification.

2.6. Intracellular reactive oxygen species (ROS) measurement

The generation of intracellular ROS was monitored using DCFH-DA [37]. The DCFH-DA passively enters into the cell where it reacts with ROS to form the highly fluorescent compound dichlorofluorescein (DCF). For the quantitative estimation of intracellular ROS by spectrofluorometry, 1×10^4 cells per well were seeded in 96-well culture plates (black-bottomed) and allowed to adhere overnight in a CO_2 incubator at 37 °C. Then, cells were treated with three different concentrations of AOAgNPs (50, 100 and 150 μg/ml) and incubated for 12 and 24 h at 37 °C. At the end of the respective treatment period, cells were washed twice with PBS and then incubated with 20 μM working solution of DCFH-DA in a serum free medium at 37 °C for 30 min. The reaction mixture was discarded and replaced by 100 μl of PBS in each well. The green fluorescence intensity was detected using a microplate reader at an excitation wavelength of 485 nm and an emission wavelength of 528 nm. The values were averaged from multiple wells and expressed as a percentage of fluorescence intensity relative to the control wells. Similarly, for the qualitative analysis of intracellular ROS by fluorescence microscopy, imaging was achieved by seeding the cells on a cover-slip-loaded 6-well plate at 1×10^5 cells/well. Then, the cells were treated and processed as indicated above. Finally, after washing with PBS, the stained cells were mounted onto a microscope slide in mounting medium and images were collected using appropriate filter settings in a compound microscope (Olympus BX41, Japan) fitted with fluorescence attachment and CCD camera.

2.7. Apoptosis induction assay by flow cytometry

Apoptosis was measured using flow cytometry to quantify the levels of detectable phosphatidylserine on the outer membrane of apoptotic cells [38]. An annexin-V FITC apoptosis detection Kit was used for the differentiation of early apoptotic, late apoptotic and necrotic cells. Briefly, MCF-7 cells at a density of 1×10^5 cells/ml were grown overnight and then incubated with 50, 100 and 150 μg/ml AOAgNPs for 24 h. All adhering cells were harvested using trypsin/EDTA solution and then washed twice with PBS before being transferred to a sterile centrifuge tube (1×10^6 cells/ml). Samples were prepared following the manufacturer instructions. Annexin-V/Propidium Iodide (PI) fluorescence was analyzed for each sample using a BD FACSCalibur flow cytometer. A total of 10,000 events were acquired for each sample and data were analyzed using Cell Quest Pro software (BD Biosciences).

2.8. Determination of DNA damage

The alkaline comet assay (Single Cell Gel Electrophoresis—SCGE) was carried out using the method described in Ateeq et al. [39], which is based on the original work of Singh et al. [40] with additional modifications. Briefly, 1×10^5 cells/well were seeded in a six-well plate and grown overnight. The MCF-7 cells were then treated with different concentrations (50, 100 and 150 μg/ml) of AOAgNPs for 24 h. After treatment, the cells were trypsinized and resuspended in cold PBS. About 15 μl of cell suspension (approximately 10,000 cells) was mixed with 100 μl of 0.75% low melting agarose at 37 °C and spread on a frosted glass slide pre- cleaned and pre-coated with a 150 μL layer of normal melting agarose (1.5%). After solidification, it was covered with a third layer of 100 μl of low melting agarose (0.75%), covered with coverslip and allowed to solidify on ice for 20 min. The coverslip was removed gently and slide was immersed in freshly prepared ice-cold lysis solution (10 mM Tris pH 10, 2.5 M NaCl, 100 mM Na_2EDTA, with 10% DMSO and 1% Triton X-100 added just before use) for 2 h at 4 °C. Following lysis treatment, slides were kept in an alkaline electrophoresis buffer (300 mM NaOH, 1 mM EDTA, pH > 13) for 20 min in a horizontal gel electrophoresis unit for DNA unwinding and conversion of alkali-labile sites to single-strand breaks. Electrophoresis was performed for 20 min by applying an electric field of 25 V and adjusting the current to 300 mA. The slides were neutralized gently with 0.4 M Tris buffer at pH 7.5. All preparative steps were conducted in the dark to prevent additional DNA damage. Each slide was stained with 75 μl of 20 μg/ml ethidium bromide solution for 3 min. The slides were analyzed under 40× objective lens (excitation wavelength of 515–560 nm and emission wavelength of 590 nm) in a compound fluorescence microscope.

The extent and distribution of DNA damage was evaluated by examining at least 300 randomly selected and non-overlapping cells (50 cells per coded slide) for each concentration in a blind analysis (six slides in each group). These cells were scored visually, according to tail size, into the following five classes: class 0—no tail; class 1—tail shorter than the diameter of the head (nucleus); class 2—tail length 1–2 times the diameter of the head; class 3—tail length more than twice the diameter of the head; class 4—no head with maximal damage. The total score for 300 comets, which ranged from 0 (all undamaged) to 1200 (all maximally damaged), was obtained by multiplying the number of cells in each class by the damage class [33,41].

2.9. Detection of autophagy by acridine orange staining

As a marker of autophagy induction, acidic vesicular organelles (AVOs), which consist predominantly of autophagosomes, and autolysosomes, were analyzed by spectrofluorometry and fluorescence microscopy after the cells were stained with acridine orange (AO) [42]. AO is a fluorescent weak base that accumulates in acidic vesicular spaces and fluoresces bright red. The intensity of the red fluorescence is proportional to the degree of AVO formation. For the quantitative estimation of autophagy, 1×10^4 cells/well were seeded in 96-well culture plates (black-bottomed) overnight, and then treated with three different concentrations of AOAgNPs (50, 100 and 150 μg/ml) and incubated for 24 h at 37 °C. Then, the cells were washed twice with PBS and incubated with 5 μg/ml working solution of AO in a serum free medium at room temperature for 15 min in the dark. The reaction mixture was discarded and replaced by 100 μl of PBS in each well. The intensity of the green fluorescence was detected using a microplate reader at an excitation wavelength of 485 nm and an emission wavelength of 528 nm. The intensity of green fluorescence was inversely proportional to the formation of AVOs since AO staining increased the red fluorescence thereby reducing the green fluorescence. The values were averaged from multiple wells and expressed as the percentage of fluorescent intensity relative to the control wells. Similarly, for the fluorescence microscopic imaging, the cells on a cover-slip-loaded six well plate were treated and processed as indicated above. Finally, the AO stained cells were observed in a fluorescence compound microscope.

2.10. Statistical analysis

All experiments were carried out with three independent replicates and values are presented as mean ± standard error of mean (SEM). Data were statistically analyzed using the Student's *t*-test for comparison between the means or using a one-way analysis of variance with a post-hoc *Dunnett's* test, and applying a significance level of $P < 0.05$.

3. Results and discussion

3.1. Biosynthesis and characterization of silver nanoparticles

In the present study, the aqueous leaf extract of *A. obesum* was used for the green-synthesis of AgNPs. After the addition of aqueous leaf extract to $AgNO_3$ solution, the color was observed to change from slight yellowish to brown (Fig. 1B,C) over a period of 120 min, indicating that the *A. obesum* leaf extract speeds up the biosynthesis of AgNPs, which is consistent with previous reports [43–45]. The color change is due to the excitation of surface plasmon vibrations with the AgNPs [46]. UV–vis spectroscopy is a valuable tool for structural characterization of AgNPs. It is well known that the optical absorption spectra of metal nanoparticles are dominated by surface plasmon resonances (SPRs) that shift to longer wavelengths with increasing particle size due to the capping agent [47,48]. It is also well recognized that the absorbance of AgNPs mainly depends upon their size and shape [49]. In general, the number of SPR peaks decreases as the symmetry of the nanoparticle increases [50]. The UV–vis spectra of AgNPs synthesized by *A. obesum* exhibit distinct peak at 425 nm, which is surface plasmon resonance of AgNPs (Fig. 1D). The UV–vis spectrum recorded after 24 h showed that there was no increase in the absorption, confirming the completion of the AgNPs synthesis reaction. The stability of the reaction solution was examined for a month by UV–vis spectroscopy and it was found that the nanoparticles continued to exhibit a peak at the same wavelength with a similar absorption intensity, confirming their stability. Similar results have also been reported in AgNPs synthesized using leaf extracts of *Mimusops elengi* [51].

Currently, the exact mechanism of silver nanoparticles biosynthesis by plant extracts is not yet fully understood. Only participation of phenolics, proteins and reducing agents in their synthesis has been speculated [52]. The reduction and stabilization of silver ions by combination of biomolecules in the plant extracts such as proteins, amino acids, enzymes, polysaccharides, alkaloids, tannins, phenolics, saponins, terpinoids and vitamins which are already established [53]. In the biosynthesis of AgNPs, capping agents are used which are absorbed by NPs. These capping agents are usually organic molecules used to aid stabilization of NPs [18].

A. obesum is a rich source of cardiac glycosides that exhibit a broad spectrum of biological activities. Fifty chemical constituents have previously been reported from different parts of *A. obesum*, belonging to cardenolides, pregnanes, triterpenes and flavonoids [21]. FTIR measurements were carried out to identify the potential biomolecules in the *A. obesum* leaf that are responsible for reduction and capping of the bioreduced AgNPs. The FTIR spectra (Fig. 2) showed certain common absorption bands at 3398 cm^{-1} that are characteristic of υ (O—H) and υ (N—H) vibrational frequencies. Vibrational peaks between 2899 and 2977 cm^{-1} were character-

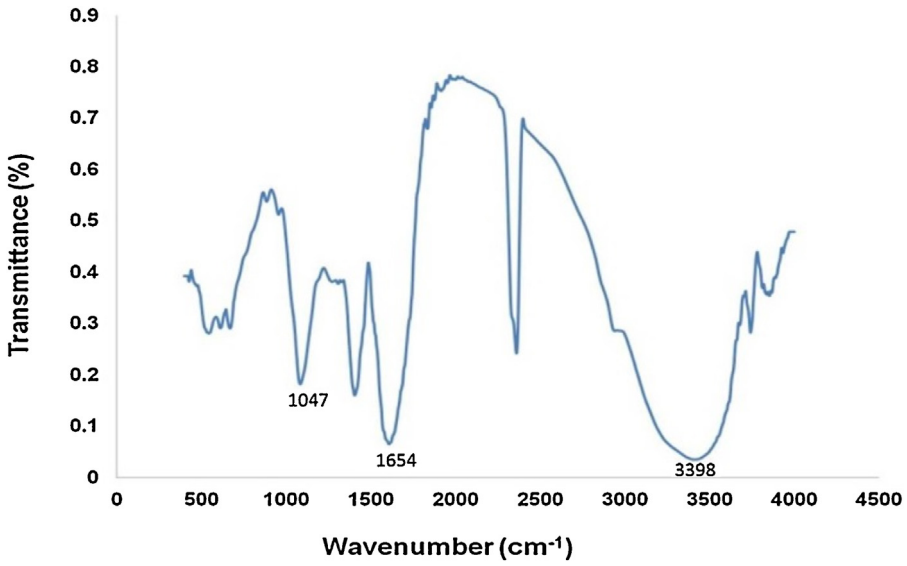

Fig. 2. FTIR spectrum of silver nanoparticles synthesized using leaf extracts of *A. obesum*.

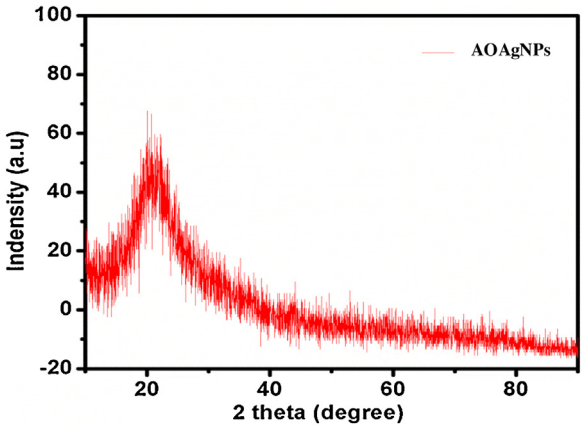

Fig. 3. XRD pattern of biosynthesized AOAgNPs exhibiting the facets of crystalline silver.

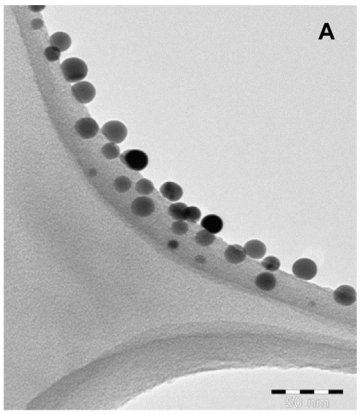

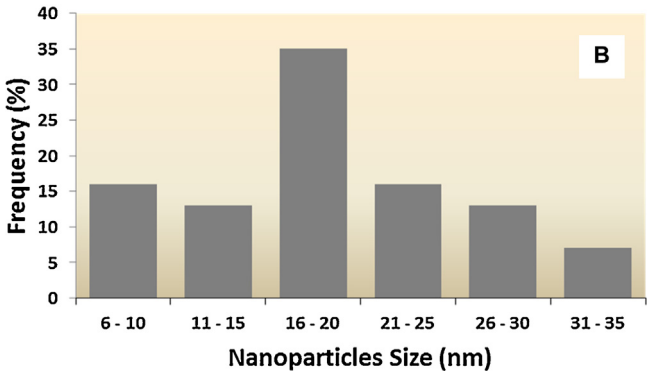

Fig. 4. (A) Representative transmission electron microscopy image of silver nanoparticles after bioreduction with leaf extract of *A. obesum*. Several fields were photographed and used to determine the diameter of the NPs. The images revealed mostly spherical particles in the size range of 10–30 nm (B).

istic of a υ (C—H) symmetrical vibration of saturated hydrocarbon. The vibrational frequency υ (C—O) was observed in the spectra of the extracts at 1047 and 1087 cm^{-1}. Deviation from this region to a higher wave number was observed, which was indicative of a secondary amide. These peaks were sharper than the υ (O—H) peaks due to a reduction in hydrogen bonds which increased with electronegativity. Vibrational peaks at 1654 cm^{-1} in the extract signified the possibility of an aromatic compound. Based on the physical state of the extract and the characteristic features of the infrared vibrational peaks in the spectra, terpenoids, long chain fatty acids, secondary amide derivatives and proteins were the possible compounds on the surface of the obtained NPs. It has been reported that proteinaceous materials and polyphenols probably serve as a capping and/or stabilizing agents for the metal NPs [18,54].

The crystalline nature of the AOAgNPs was confirmed by XRD analysis. The XRD patterns of the lyophilized AOAgNPs are shown in Fig. 3. Intense peaks were observed at 38° and 43.7° in the 2θ range, which correspond to the (1 1 1) and (2 0 0) reflection planes of the face-centred cubic (fcc) structure of Ag planes (JCPDS card file no. 04-0783). The results of the XRD pattern further corroborate the synthesis of AgNPs, with the sharp bands typical of Bragg peaks, which may be due to the stabilization of the synthesized nanoparticles by the various reducing agents present in the *A. obesum* leaf extract, thus providing for the crystallinity of the silver nanoparticles [55].

The TEM micrographs of AOAgNPs reveal polydisperse NPs, most of which have a spherical morphology, with a size range of 10–30 nm. Particle size analysis for 300 NPs revealed homogeneous distribution with about 35% of NPs were in the size range of 16–20 nm (Fig. 4A–B). The synthesis of NPs through green approaches provides a flexible control over the size and shape of

the nanoparticles [56]. In fact, the diversity in the concentration and composition of the biologically active components of plant extracts and the types of metal salts, the ability to alter the composition of a reaction mixture and reaction conditions through changes in the temperature, pH, and inclusion of additives of biological origin (biomatrices), serve to control the size and morphology of nanostructures [56].

3.2. Cytotoxicity of AOAgNPs by MTT assay

The cytotoxic activity of AOAgNPs to MCF-7 cells was determined by using the MTT assay, which can provide information on cell death, survival and metabolic activities. MCF-7 cells were treated with concentrations of AOAgNPs in ranging 100–600 μg/ml for 24 h. A dose-dependent decrease in the percentage of cell viability was observed in the range of 18–83% with increased concentration of AOAgNPs. An IC_{50} value of 217 μg/ml was obtained (Fig. 5A); and hence, three concentrations below the IC_{50} value (50, 100, 150 μg/ml) were used in all subsequent assays. In contrast, the crude aqueous leaf extract showed milder cytotoxicity, with the cell viability being decreased to 46% at the highest concentration of 600 μg/ml. An IC_{50} value of 580 μg/ml was calculated for the crude leaf extract (Fig. 5A). Cytotoxicity test was also conducted by using commercial AgNPs produced using non-green method. The results revealed a concentration dependent decrease in the viability of MCF-7 cells from 79% to 29% through 20 μg/ml to 120 μg/ml concentrations, respectively. The IC_{50} value was estimated at 73 μg/ml (Fig. 5B). These findings suggest that plant bio components increased AgNPs biocompatibility by reducing the toxicity of AgNPs (IC_{50} 73 μg/ml) when compared to the toxicity of AOAgNPs (IC_{50} 217 μg/ml). On the other hand, the synthesized AOAgNPs increased the anticancer potential of crude *A. obesum* leaves extract (IC_{50} 580 μg/ml), suggesting that biosynthesized AgNPs will contribute to find alternative chemotherapeutic agent. The exact mechanism involve in the variations in the above cytotoxic effects is not clear. The cytotoxic effects induced by AOAgNPs is mainly attributed to AgNPs but plant components attached to the AOAgNPs somehow modulated its toxicity.

The MCF-7 cell line has been used previously for various cytotoxicity studies with AgNPs and plant extract based AgNPs [17,57]. Moreover, a large number of *in vitro* studies have indicated that AgNPs are toxic to mammalian cells [58–59]. Our results also provide conclusive evidence for the cytotoxic effect of biosynthesized AgNPs using *A. obesum* against the breast cancer MCF-7 cell line by decreasing the progressive development of cancer cells.

3.3. Analysis of morphological changes by phase contrast microscopy

The representative image of morphological changes observed under phase contrast inverted microscopy in MCF-7 cells after exposure to 150 μg/ml AOAgNPs for 24 h is shown in Fig. 5D. No significant changes in the morphology were observed in control cells (Fig. 5C). The cells appeared to have a normal shape, were attached to the surface and reached about 95–100% confluence. Conversely, the characteristics of apoptotic cell death were evident in AOAgNPs treated MCF-7 cells, where cell shrinkage, loss of cell adhesion, decreased cell density, along with incorporation of NPs, were clearly observed. The cytotoxic effect of AOAgNPs may be attributed to high content of cardiac glycosides found in *A. obesum* [21] that might have involved in the reduction process of AOAgNPs. Cardiac glycosides have anti-neoplastic properties and the ability to induce cell death through several supposed molecular mechanisms, like: activation of intrinsic pathway of apoptosis, autophagy, and generation of ROS [60,61].

These findings concord with increasing concern about the use of nanomaterials in consumer and industrial products due to their toxicity and their uncertain fate in biological systems [59]; *in vitro* studies have reported that AgNPs produced toxicity targeted at a variety of organs including the lung, liver, brain, vascular system and reproductive organs. AgNPs have also been shown to induce the expression level of genes involved in cell cycle progression and apoptosis [58].

3.4. Determination of intracellular reactive oxygen species (ROS)

ROS play an important role in a variety of normal biochemical functions, and alterations in their activity leads to pathological conditions. NPs have been shown to enhance the intracellular ROS level in many cell lines. To investigate the potential role of AOAgNPs in inducing oxidative stress in MCF-7 cells, therefore, intracellular ROS generation was measured by HDCF-DA assay using fluorescence microscopy and spectrofluorometry. As shown in Fig. 6(A–D), after 24 h exposure to AOAgNPs, an increase in the ROS level was observed in a concentration dependent manner, as reflected by the enhanced intensity of the green fluorescence compared to the control. This pattern was also confirmed by quantitative estimation of fluorescent intensity, where a significant increase ($p < 0.05$) in the ROS level was recorded (Fig. 6E). Compared to the control group, a maximum of 2.4 and 1.7 fold increases in ROS generation was observed in a 150 μg/ml concentration of AOAgNPs after 24 h and 12 h treatments, respectively. Moreover, consistent with previous reports that nanomaterials provoke oxidative stress [62,63], the present results also showed that AOAgNPs induced ROS generation.

Environmental toxicants are known to induce oxidative stress and alterations in the cellular redox balance. Oxidative stress in turn plays an important role in many types of cellular injury, some of which can result in DNA damage, apoptotic cell death and autophagy [31,64]. It is now well established that AgNPs generate the formation of ROS, leading to oxidative stress and cytotoxicity. Many studies have implicated intracellular ROS in the signal transduction pathways leading to apoptosis [65,66]. It has also been reported that apoptosis induced by exposure to AgNPs was mediated by oxidative stress in fibroblast, muscle and colon cells [67,68].

3.5. Apoptosis analysis by Annexin V/PI binding

We quantified the extent of apoptosis in cells labeled with Annexin-V/PI staining using flow cytometry. Representative dot plots showed that, for the control group, only 2–5% cells were dead or undergoing apoptosis, which is a normal event for cells growing in cultures. After exposure to AOAgNPs, however, the proportion of early and late apoptotic cells increased significantly ($P < 0.05$) as compared with control cells at any dose for 24 h (Fig. 7A). There were no changes registered in the percentage of necrotic cell death. A concentration dependent increase in the percentage of early and late apoptotic cells were observed with values of about 4–18% and 11–24%, between 50 μg/ml and 150 μg/ml AOAgNPs concentrations, respectively (Fig. 7B). Recent reports have also identified apoptosis as a major mechanism of cell death in exposure to nanomaterials [68,69]; however, conflicting results suggest the involvement of additional parameters in nanoparticle-mediated cell death [70,71].

3.6. DNA damage detection by comet assay

The ability of AOAgNPs to damage DNA in the MCF-7 cells was evaluated by alkaline comet assay. The results are presented in Fig. 8, and show the DNA damage (according to tail length) in MCF-7 cells exposed to three different concentrations for 24 h. AOAgNPs

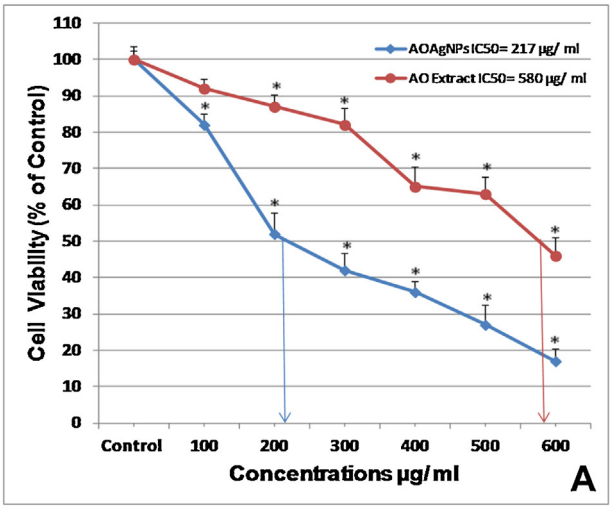

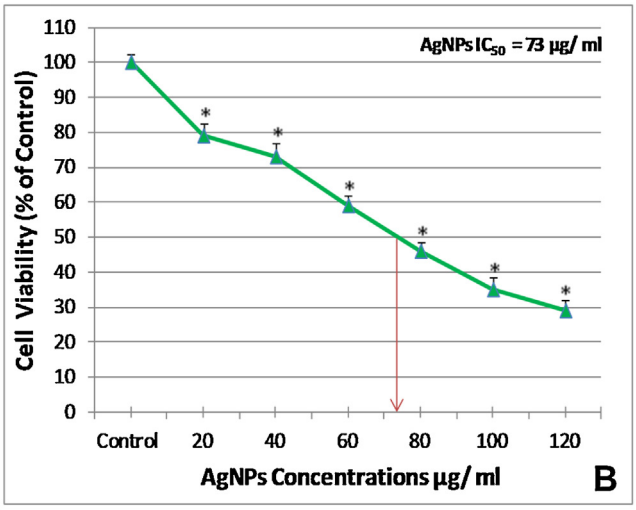

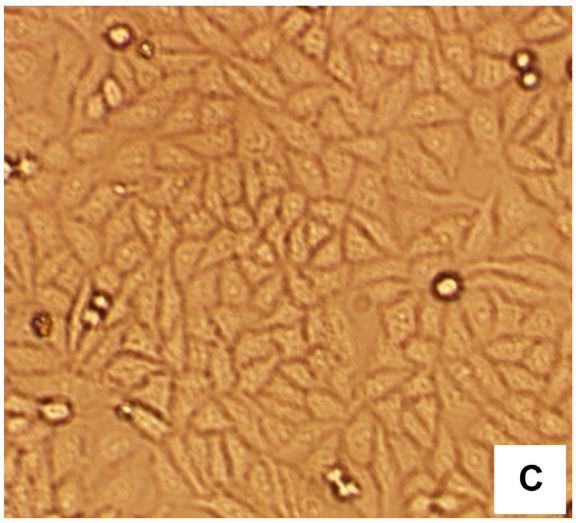

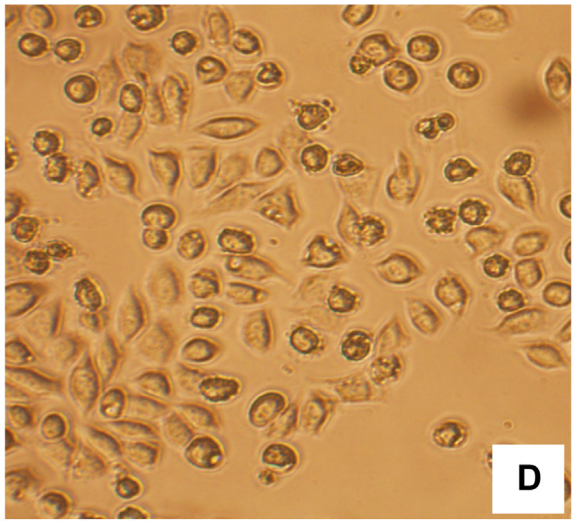

Fig. 5. (A) Cell viability was determined by MTT assay. MCF-7 cells were exposed to different concentrations of AOAgNPs and crude leaves extract (100–600 µg/ ml) for 24 h, after which the formazan product was quantified by spectrophotometry. A clear dose-dependent cytotoxic effect was observed with increasing concentration of AOAgNPs. An IC_{50} value of 217 µg/ml and 580 µg/ml was estimated for AOAgNPs and crude leaves extract, respectively. (B) A dose dependent decrease in cell viability was evident at the indicated concentrations of AgNPs. The IC_{50} value was estimated at 73 µg/ml. (*Significant, $p < 0.05$). Morphological changes were observed in MCF-7 cells after exposure to 150 µg/ml AOAgNPs for 24 h. Untreated cells appeared normal in shape, with about 95–100% confluency (C), while loss of cell adhesion, decreased cell density along with incorporation of AOAgNPs into cells was visualized in the treated sample (D), (magnification 100×).

Table 1
Shows the extent of DNA damage in the form of comet class (measure of comet tail length). Total comet score (TCS) was calculated by the method mentioned in the materials and methods section.

Treatments (µg/ml)	No. of cells observed	Comets per damage class					Total comet score (TCS)
		0	1	2	3	4	
Control	300	277	21	2	0	0	25
Dox (50 µM)	300	221	61	8	10	0	107*
50	300	220	80	6	1	0	95*
100	300	196	82	13	9	0	135*
150	300	170	98	19	8	5	180*

* Significant ($p < 0.05$).

were significantly genotoxic to the MCF-7 cells, as noted by the concentration dependent increase in DNA fragmentation. Microscopic images confirmed that comet tail lengths were significantly longer in treated cells (Fig. 8B–D) as compared to control cells (Fig. 8A). Furthermore, to quantify and distinguish different DNA damage levels, an evaluation of the total comet score (TCS) was performed. The TCS for each experimental group, including positive and negative controls are presented in Table 1 and Fig. 8E. All concentrations of AOAgNPs induced statistically significant ($p < 0.05$) DNA damage after 24 h of treatment. The maximum comet score of 180 was estimated in the 150 µg/ml treatment group, compared to 25 in the negative control group. At lower concentration, most of the damage was minor (class 1), but cells treated with high concentrations showed extensive damage (class 2 and 3), while the control groups contained mostly undamaged cells (class 0).

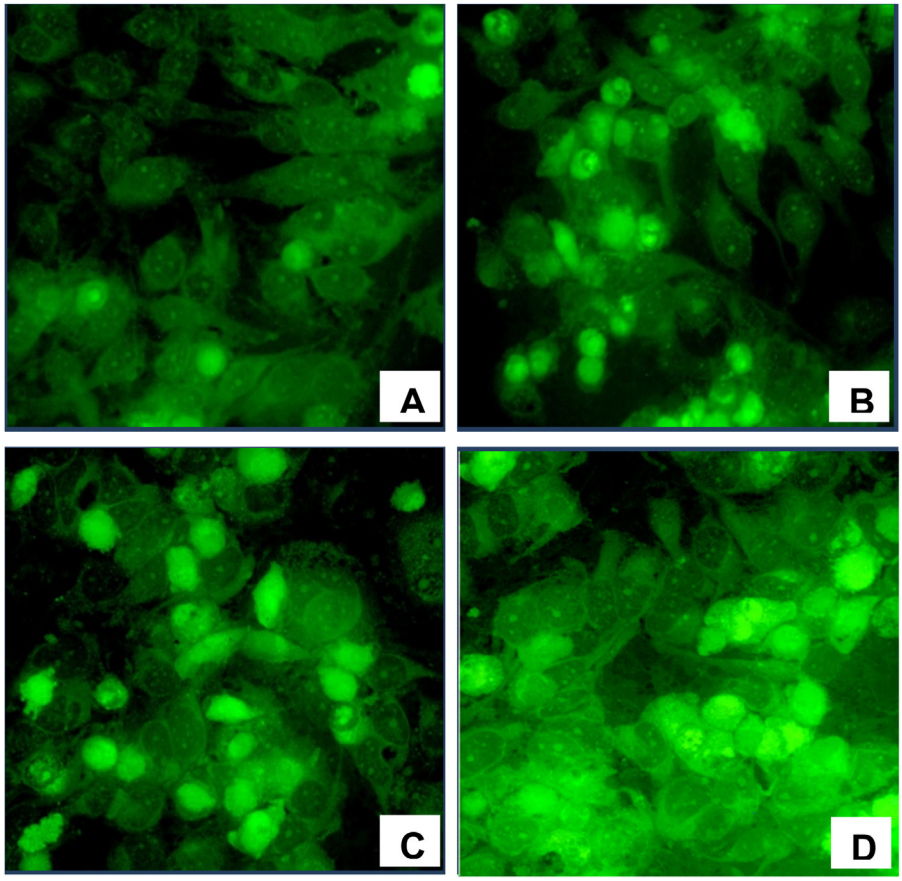

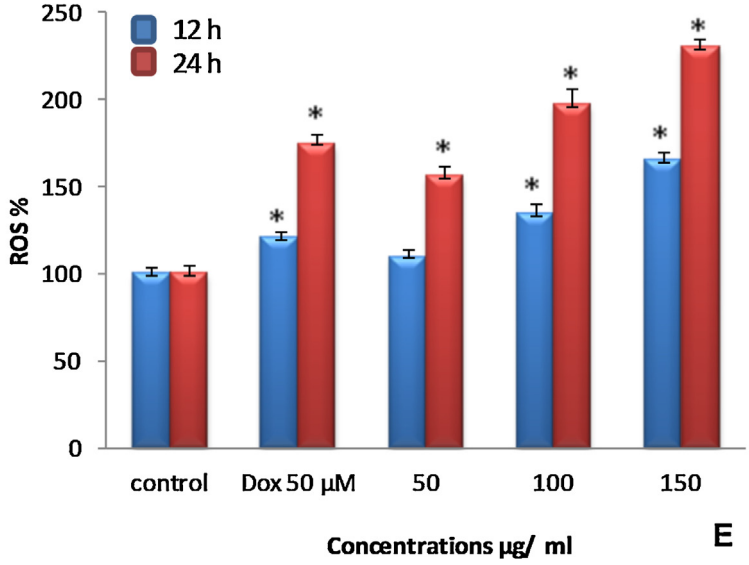

Fig. 6. Detection of intracellular ROS by the measurement of fluorescent intensity and fluorescence microscopy (A–D). MCF-7 cells were exposed to different concentrations of AOAgNPs for 12 and 24 h and the cells were then incubated with 10 µM DCF-DA for 20 min followed by washing. They were examined by fluorescence microscopy using a blue filter. Representative images of cells treated for 24 h from three independent experiments are shown. (E) Fluorescent intensities were measured for green fluorescence (excitation = 485 nm, emission = 530 nm). The values are expressed as mean ± SE, (*Significant, $p < 0.05$).

Highly reactive hydroxyl radicals attack cellular components including DNA, lipids, and proteins to cause various kinds of oxidative damage [72,73]. AgNPs have been found to increase the DNA tail length in a comet assay, which measures DNA strand breaks, as well as alkali labile sites [74,75]. AgNPs induced DNA breakage was also detected in cell lines using the comet assay [76,77].

3.7. Detection of autophagy by acridine orange staining

Autophagy is a physiologically regulated process that, under certain stress conditions, allows degradation of the cytoplasmic contents including unfolded proteins and membranous organelles [78]. There is an increasing body of evidence showing a link

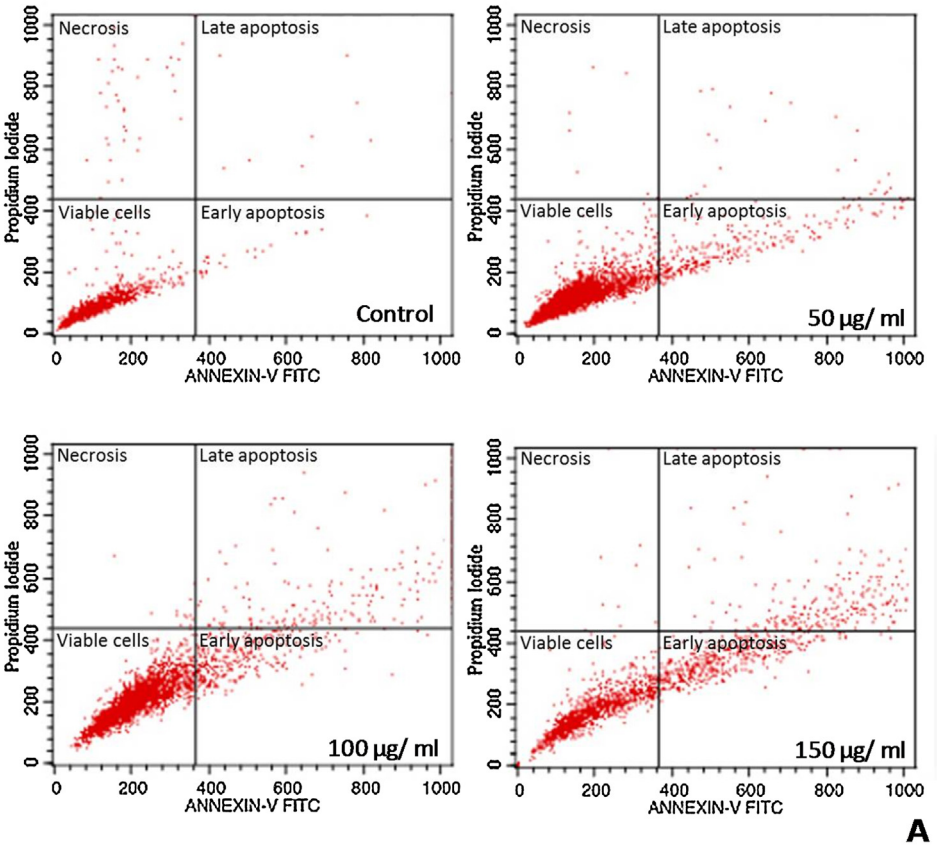

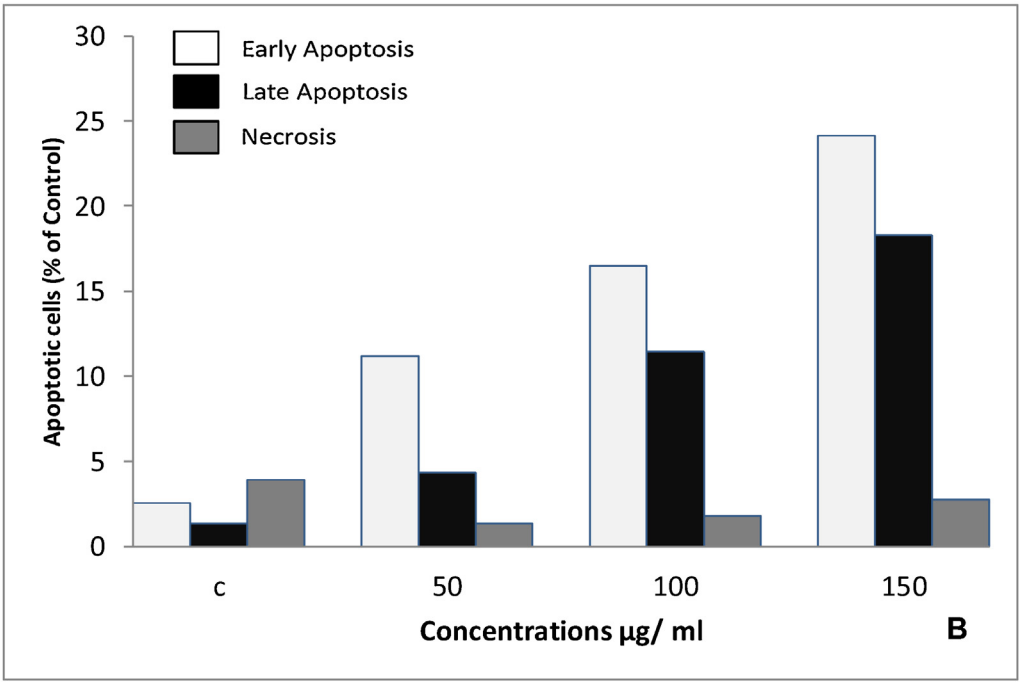

Fig. 7. Flow cytometry analysis to determine the PS translocation in MCF-7 cells (Annexin V–FITC assay). MCF-7 cells were harvested after the desired treatment, incubated with Annexin V/PI and analyzed by flow cytometry. (A) Representative dot plots are shown where the percentage of viable cells, early apoptosis, late apoptosis and necrosis cells are evident after exposure to different concentrations of AOAgNPs. (B) The data were represented as mean ± SE from three independent experiments. A dose-dependent increase in apoptosis was observed in treated cells.

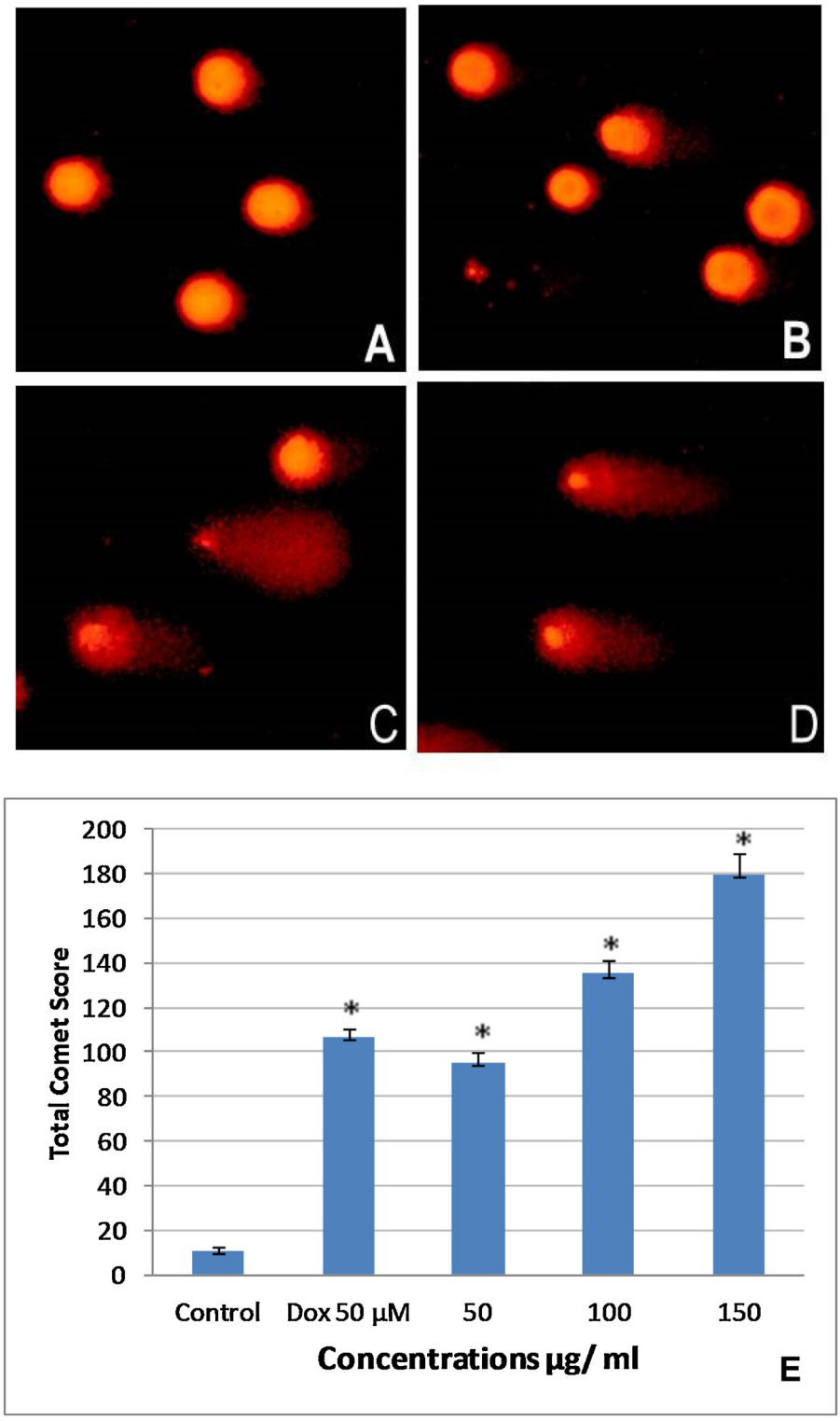

Fig. 8. DNA-damage evaluations by comet assay in MCF-7 cells after treatment with AOAgNPs for 24 h. Representative images of different classes of comets are shown. (A) Control with no damage, (B) 50 µg/ml with minimal damage, (C) 100 µg/ml with average damage, and (D) 150 µg/ml with higher damage, respectively. The total comet score was calculated as mentioned in the materials and methods section and presented as mean ± SE from three independent experiments (E), (*Significant, $p < 0.05$).

between ROS and autophagy, in which ROS generation could trigger autophagy [31]. In the present study, therefore, we sought to elucidate the role of ROS and autophagy in determining the fate of AOAgNPs treated MCF-7 cells. Acridine orange was used to detect the acidic vesicular organelles (AVOs). Concentrated AO in the vesicles fluoresces bright red, whereas the cytoplasm and the nucleus show a dominant green fluorescence. Staining of MCF-7 cells revealed the appearance of AVOs after treatment with AOAgNPs for 24 h. Fluorescence microscopy images revealed that untreated cells exhibited limited AVOs in the cytoplasm and showed green fluorescence with minimal red fluorescence (Fig. 9A). On the contrary, the majority of the cells treated with AOAgNPs exhibited more AVOs

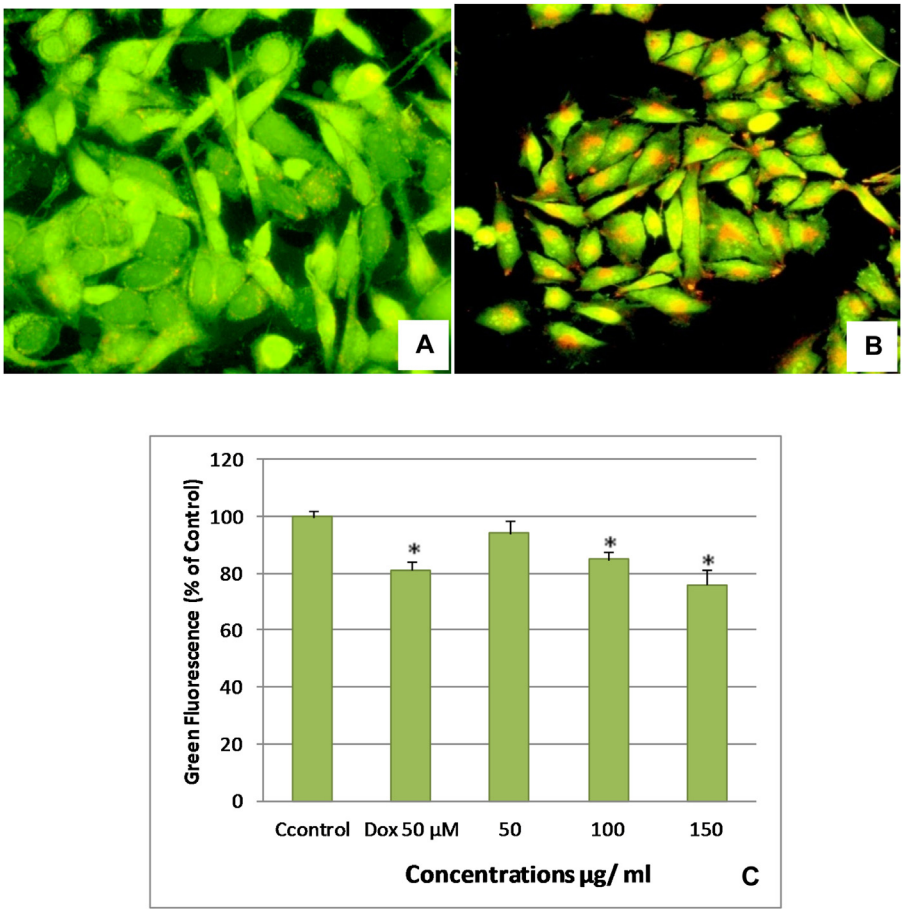

Fig. 9. Induction of autophagy was determined by fluorescence microscopy after acridine orange staining in MCF-7 cells treated with AOAgNPs for 24 h. (A) control cells with no red fluorescence, (B) treated cells displayed extensive red fluorescence in the cytoplasm which represents acidic vesicular organelles (AVO). The formation of AVOs was quantified by spectrofluorometry (C). A decrease in green fluorescence was observed in treated cells due to the formation of AVOs. The data were presented as mean ± SE from three independent experiments, (*Significant, $p < 0.05$).

in the perinuclear region of the cytoplasm (Fig. 9B). Quantitative analysis of AO staining verified that AOAgNPs triggered a significantly higher percentage of cells with AO than the untreated group after 24 h exposure, since the intensity of green fluorescence was reduced (Fig. 9C).

It has been suggested that the cells exposed to excessive ROS due to treatment with AgNPs may have impaired autophagic function, resulting in the accumulation of damaged organelles, such as mitochondria, which can induce oxidative stress, inflammation and DNA damage [59]. Autophagy dysfunction is recognized as a potential mechanism of cell death, resulting in either apoptosis or autophagic cell death [79]. Previous studies have demonstrated that nanoparticles from various sources [80–82] including AgNPs [59], can induce autophagosome accumulation in treated cells. Cancer cells, with their higher metabolic rate, even at basal conditions, would result in high intracellular ROS concentrations. This in turn puts cancer cells under increased oxidative stress, making them more vulnerable to ROS-mediated attack and cell death [83]. ROS selectively target malignant in preference to normal cells for induction of autophagy, a fact that has important implications for anticancer therapy [78]. The role played by autophagy in cell death is of great interest because the potential ability of autophagy to modulate cell death makes it a therapeutic target in several diseases, including cancer and neurodegeneration [84].

4. Conclusions

This investigation has demonstrated the potential of *A. obesum* as a biological reducing agent and capping agent for the synthesis of AgNPs. This approach has several advantages which provide for the combined use of two anticancer agents (*A. obesum* leaves extract and AgNPs) at low cost and short time. AOAgNPs were able to reduce the viability of the MCF-7 cells in a dose-dependent manner. Furthermore, AOAgNPs enhanced the intracellular levels of ROS and induced DNA damage, apoptosis and autophagy. Moreover, the IC_{50} value of AOAgNPs (217 µg/ml) was found to be reduced compared to that of the crude extract (580 µg/ml), whereas AgNPs were found to be toxic at very low concentrations (IC_{50} 73 µg/ml). These results suggest that the capping agent from *A. obesum* increases the anticancer therapeutic potential of crude extract as well as biocompatibility of AgNPs by reducing its toxicity. These findings will find its application in modulating the general toxicity of AgNPs produced using non-green method. Biosynthesized AgNPs could play an important role in improving their bioavailability as well as compatibility for therapeutical applications in disease like cancer. The exact mechanism through which AOAgNPs exert their effects on MCF-7 cells is not fully understood. Further *in vitro* studies are required to elucidate the precise mechanism and to ascertain if the effects of AOAgNPs are consistent in other cancerous cell lines.

Conflict of interest

The authors report no conflicts of interest in this work.

Acknowledgement

The authors extend their appreciation to the Deanship of Scientific Research at King Saud University for funding the work through the research group project No RGP-VPP-195.

References

[1] J. Su, J. Zhang, L. Liu, Y. Huang, R.P. Mason, J. Nanosci. Nanotechnol. 8 (2008) 1174–1177.
[2] T.M. Tolaymat, A.M. El Badawy, A. Genaidy, K.G. Scheckel, T.P. Luxton, M. Suidan, Sci. Total Environ. 408 (2010) 999–1006.
[3] R. Vaidyanathan, K. Kalishwaralal, S. Gopalram, S. Gurunathan, Biotechnol. Adv. 27 (2009) 924–937.
[4] S. Moaddab, H. Ahari, D. Shahbazzadeh, A.A. Motallebi, A.A. Anvar, J. Rahman-Nya, M.R. Shokrgozar, Int. Nano Lett. 1 (2011) 6.
[5] L. Xu, X. Li, T. Takemura, N. Hanagata, G. Wu, L.L. Chou, J. Nanobiotech. 10 (2012) 1–11.
[6] M. Ghosh, J. Manivannan, S. Sinha, A. Chakraborty, S.K. Mallick, M. Bandyopadhyay, A. Mukherjee, Mutat. Res. 749 (2012) 60–69.
[7] R. Sukirtha, K. Priyanka, J.J. Antony, S. Kamalakkannan, R. Thangam, P. Gunasekaran, K. Muthukalingan, A. Shanmugam, Process Biochem. 47 (2012) 273–279.
[8] R.R. Naik, S.J. Stringer, G. Agarwal, S. Jones, M.O. Stone, Adv. Funct. Mater. 14 (2002) 25–30.
[9] Y. Sun, Y. Yin, B.T. Mayers, T. Herricks, Y. Xia, Chem. Mater. 14 (2002) 4736–4745.
[10] B. Yin, H. Ma, S. Wang, S. Chen, J. Phys. Chem. B 107 (2003) 8898–8904.
[11] A. Callegari, D. Tonti, M. Chergui, Nano Lett. 3 (2003) 1565–1568.
[12] B. Ankamwar, C. Damle, A. Ahmad, M. Sastry, J. Nanosci. Nanotechnol. 5 (2005) 1665–1671.
[13] R. Geethalakshmi, D.V. Sarada, Int. J. Nanomed. 7 (2012) 5375–5384.
[14] M. Ghaffari-Moghaddam, R. Hadi-Dabanlou, M. Khajeh, M. Rakhshanipour, K. Shameli, Korean J. Chem. Eng. 31 (2014) 548–557.
[15] N.H. Mohamed, M.A. Ismail, W.M. Abdel-Mageed, A.A.M. Shoreit, Asian Pac. J. Trop. Biomed. 4 (2014) 876–883.
[16] M. Mano Priya, B.K. Selvi, J.A. John Paul, Dig. J. Nanomater. Bios. 6 (2011) 869–877.
[17] R. Vivek, T. Ramar, M. Krishnasamy, G. Palani, K. Krishnasamy, K. Soundarapandian, Process Biochem. 47 (2012) 2405–2410.
[18] F.S. Rosarin, V. Arulmozhi, S. Nagarajan, S. Mirunalini, Asian Pac. J. Trop. Med. 6 (2013) 1–10.
[19] R. Govender, A. Phulukdaree, R.M. Gengan, K. Anand, A.A. Chuturgoon, J. Nanobiotech. 11 (2013) 5.
[20] S. Arokiyaraj, V.A. Mariadhas, V. Savariar, U.P. Nyayirukannaian, H.C. Seong, O. Young-Kyoon, C.C. Ki, H.K. Kyoung, Int. J. Nanomed. 9 (2014) 379–388.
[21] M.A. Versiani, S.K. Ahmed, A. Ikram, S.T. Ali, K. Yasmeen, S. Faizi, Chem. Biodivers. 11 (2014) 171–180.
[22] T. Yamauchi, F. Abe, Chem. Pharm. Bull. 38 (1990) 669–672.
[23] H. Almehdar, H.M. Abdallah, A.M. Osman, E.A. Abdel-Sattar, J. Nat. Med. 66 (2012) 406–412.
[24] H. Kiyohara, C. Ichino, Y. Kawamura, T. Nagai, N. Sato, H. Yamada, M.M. Salama, E. Abdel-Sattar, Phytomedicine 19 (2012) 111–114.
[25] D.D. Gan, M. Macaluso, C. Cinti, K. Khalili, J. Exp. Clin. Cancer Res. 22 (2003) 509–516.
[26] ACS, Cancer Facts & Figs. 2011–2012. Atlanta : American Cancer Society, Inc. (2014).
[27] C.E. DeSantis, C.C. Lin, A.B. Mariotto, R.L. Siegel, K.D. Stein, J.L. Kramer, R. Alteri, A.S. Robbins, A. Jemal, CA: Cancer J. Clin. 64 (2014) 252–271.
[28] D.W. Kim, G.H. Hong, H.H. Lee, S.H. Choi, B.G. Chun, C.K. Won, I.K. Hwang, M.H. Won, Neuroscience 117 (2007) 387–400.
[29] P.V. AshaRani, G. Low Kah Mun, M.P. Hande, S. Valiyaveettil, ACS Nano 3 (2009) 279–290.
[30] R. Foldbjerg, P. Olesen, M. Hougaard, D.A. Dang, H.J. Hoffmann, H. Autrup, Toxicol. Lett. 190 (2009) 156–162.
[31] R. Scherz-Shouval, Z. Elazar, Trends Cell Biol. 17 (2007) 422–427.
[32] R.R. Tice, E. Agurell, D. Anderson, B. Burlinson, A. Hartmann, H. Kobayashi, Y. Miyamae, E. Rojas, J.C. Ryu, Y.F. Sasaki, Environ. Mol. Mutagen. 35 (2000) 206–221.
[33] A.R. Collins, Mol. Biotechnol. 26 (2004) 249–260.
[34] R.C. Murdock, L. Braydich-Stolle, A.M. Schrand, J.J. Schlager, S.M. Hussain, Toxicol. Sci. 101 (2008) 239–253.
[35] W. Strober, Curr. Protoc. Immunol. (2001), A.3B.1–A.3B.2.
[36] T. Mosmann, J. Immunol. Methods 65 (1983) 55–63.
[37] H. Wang, J.A. Joseph, Free Radic. Biol. Med. 27 (1999) 612–661.
[38] A.M. Evens, S. Prachand, B. Shi, M. Paniaqua, L.I. Gordon, R.B. Gartenhaus, Clin. Cancer Res. 10 (2004) 1481–1491.
[39] B. Ateeq, M. Abul Farah, W. Ahmad, Ecotox. Environ. Saf. 62 (2005) 348–354.
[40] N.P. Singh, M.T. McCoy, R.R. Tice, E.L. Schneider, Exp. Cell Res. 175 (1988) 184–191.
[41] A. Azqueta, Y. Lorenzo, A.R. Collins, Mutagenesis 24 (2009) 379–381.
[42] S. Paglin, T. Hollister, T. Delohery, N. Hackett, M. McMahill, E. Sphicas, D. Domingo, J. Yahalom, Cancer Res. 61 (2001) 439–444.
[43] J.Y. Song, B.S. Kim, Bioprocess. Biosyst. Eng. 32 (2009) 79–84.
[44] C. Krishnaraj, E.G. Jagan, S. Rajasekar, P. Selvakumar, P.T. Kalaichelvan, N. Mohan, Colloids Surf. B: Biointerfaces 76 (2010) 50–56.
[45] A.D. Dwivedi, K. Gopal, Colloid Surf. A: Physicochem. Eng. Aspect 369 (2010) 27–33.
[46] P. Mulvaney, Langmuir 12 (1996) 788–800.
[47] R. Brause, H. Moeltgen, K. Kleinermanns, Appl. Phys. B: Lasers Opt. 75 (2002) 711–716.
[48] C.R.K. Rao, D.C. Trivedi, Mater. Chem. Phys. 99 (2006) 354–360.
[49] J.J. Mock, M. Barbic, D.R. Smith, D.A. Shultz, S. Shultz, J. Chem. Phys. 116 (2002) 6755–6759.
[50] I.O. Sosa, C. Noguez, R.G. Barrera, J. Phys. Chem. B 107 (2003) 6269–6275.
[51] P. Prakash, P. Gnanaprakasam, R. Emmanuel, S. Arokiyaraj, M. Saravanan, Colloids Surf. B: Biointerfaces 108 (2013) 255–259.
[52] K. Satyavani, S. Gurudeeban, T. Ramanathan, T. Balasubramanian, J. Nanobiotechnol. 9 (2011) 43.
[53] N. Kulkarni, U. Muddapur, J. Nanotechnol. (2014) 1–8.
[54] A.K. Suresh, D.A. Pelletier, W. Wang, J.W. Moon, B. Gu, N.P. Mortensen, D.P. Allison, D.C. Joy, T.J. Phelps, M.J. Doktycz, Environ. Sci. Technol. 44 (2010) 5210–5215.
[55] N. Asmathunisha, K. Kathiresan, R. Anburaj, M.A. Nabeel, Colloids Surf. B: Biointerfaces 79 (2010) 488–493.
[56] V.V. Makarov, A.J. Love, O.V. Sinitsyna, S.S. Makarova, I.V. Yaminsky, M.E. Taliansky, N.O. Kalinina, Acta Nat. 6 (2014) 35–44.
[57] M.A. Franco-Molina, E. Mendoza-Gamboa, C.A. Sierra-Rivera, R.A. Gómez-Flores, P. Zapata-Benavides, P. Castillo-Tello, J.M. Alcocer-González, D.F. Miranda-Hernández, R.S. Tamez-Guerra, C. Rodríguez-Padilla, J. Exp. Clin. Cancer Res. 29 (2010) 148.
[58] M. Ahamed, M.S. Alsalhi, M.K. Siddiqui, Clin. Chim. Acta 411 (2010) 1841–1848.
[59] Y.H. Lee, F.Y. Cheng, H.W. Chiu, J.C. Tsai, C.Y. Fang, C.W. Chen, Y.J. Wang, Biomaterials 35 (2014) 4706–4715.
[60] Y. Wang, Q. Qiu, J.J. Shen, D.D. Li, X.J. Jiang, S.Y. Si, R.G. Shao, R.G.Z. Wang, Int. J. Biochem. Cell Biol. 44 (2012) 1813–1824.
[61] R.A. Newman, P. Yang, H.N. Hittelman, T. Lu, D.H. Ho, D. Ni, D. Chan, M. Vijjeswarapu, C. Cartwright, S. Dixon, E. Felix, C. Addington, J. Exp. Ther. Oncol. 5 (2006) 167–181.
[62] L. Harhaji, A. Isakovic, N. Raicevic, Z. Markovic, B. Todorovic-Markovic, N. Nikolic, S. Vranjes-Djuric, I. Markovic, V. Trajkovic, Eur. J. Pharmacol. 568 (2007) 89–98.
[63] L.K. Limbach, P. Wick, P. Manser, R.N. Grass, A. Bruinink, W.J. Stark, Environ. Sci. Technol. 41 (2007) 4158–4163.
[64] S. Kim, D.Y. Ryu, J. Appl. Toxicol. 33 (2013) 78–89.
[65] S. Ueda, H. Masutani, H. Nakamura, T. Tanaka, M. Ueno, J. Yodoi, Antioxid. Redox. Sign. 4 (2002) 405–414.
[66] M. Ott, V. Gogvadze, S. Orrenius, B. Zhivotovsky, Apoptosis 12 (2007) 913–922.
[67] D.R. Green, J.C. Reed, Science 281 (1988) 1309–1312.
[68] Y.H. Hsin, C.F. Chen, S. Huang, T.S. Shih, P.S. Lai, P.J. Chueh, Toxicol. Lett. 179 (2008) 130–139.
[69] Y. Pan, S. Neuss, A. Leifert, M. Fischler, F. Wen, U. Simon, G. Schmid, W. Brandau, W. Jahnen-Dechent, Small 3 (2007) 1941–1949.
[70] J.A. Khan, B. Pillai, T.K. Das, Y. Singh, S. Maiti, ChemBioChem 8 (2007) 1237–1240.
[71] S. Park, Y.K. Lee, M. Jung, K.H. Kim, N. Chung, E.K. Ahn, Y. Lim, K.H. Lee, Inhal. Toxicol. 19 (2007) 59–65.
[72] B. Halliwell, O.I. Aruoma, FEBS Lett. 281 (1991) 9–19.
[73] N.A. Denisova, I. Cantuti-Castelvetri, W.N. Hassan, K.E. Paulson, J.A. Joseph, Free Radic. Biol. Med. 30 (2001) 671–678.
[74] N.P. Singh, Mutat. Res. 455 (2000) 111–127.
[75] R. Rajagopalan, S.K. Ranjan, C.K. Nair, Mutat. Res. 536 (2003) 15–25.
[76] S. Hackenberg, A. Scherzed, M. Kessler, S. Hummel, A. Technau, K. Froelich, C. Ginzkey, C. Koehler, R. Hagen, N. Kleinsasser, Toxicol. Lett. 201 (2011) 27–33.
[77] M. Jeyaraj, G. Sathishkumar, G. Sivanandhan, D. Mubarak Ali, M. Rajesh, R. Arun, G. Kapildev, M. Manickavasagam, N. Thajuddin, K. Premkumar, A. Ganapathi, Colloids Surf. B: Biointerfaces 106 (2013) 86–92.
[78] C. He, D.J. Klionsky, Annu. Rev. Genet. 43 (2009) 67–93.
[79] G. Kroemer, M. Jaattela, Nat. Rev. Cancer 5 (2005) 886–897.
[80] S.T. Stern, B.S. Zolnik, C.B. McLeland, J. Clogston, J. Zheng, S.E. McNeil, Toxicol. Sci. 106 (2008) 140–152.
[81] J.J. Li, D. Hartono, C.N. Ong, B.H. Bay, L.Y. Yung, Biomaterials 31 (2010) 5996–6003.
[82] H.L. Liu, Y.L. Zhang, N. Yang, Y.X. Zhang, X.Q. Liu, C.G. Li, Y. Zhao, Y.G. Wang, G.G. Zhang, P. Yang, F. Guo, Y. Sun, C.Y. Jiang, Cell Death Dis. 2 (2011) e159.
[83] L.U. Ling, K.B. Tan, H. Lin, G.N. Chiu, Cell Death Dis. 2 (2011) e129.
[84] E.A. Corcelle, P. Puustinen, M. Jäättelä, FEBS J. 276 (2009) 6084–6096.